Frequency Domain Processing Techniques for Pulse Shape Modulated Ultra Wideband Systems

Alex Cartagena Gordillo and Ryuji Kohno

Abstract: **In this paper, two frequency domain signal processing techniques for pulse shape modulation (PSM) ultra wideband (UWB) systems are presented. Firstly, orthogonal detection of UWB PSM Hermite pulses in frequency domain is addressed. It is important because time domain detection by correlation-based receivers is severely degraded by many sources of distortion. Pulse-shape, the information conveying signal characteristic, is deformed by AWGN and shape-destructive addition of multiple paths from the propagation channel. Additionally, because of the short nature of UWB pulses, timing mismatches and synchronism degrade the performance of PSM UWB communication systems. In this paper, frequency domain orthogonality of the Hermite pulses is exploited to propose an alternative detection method, which makes possible efficient detection of PSM in dense multipath channel environments. Secondly, a ranging method employing the Cepstrum algorithm is proposed. This method is partly processed in the frequency domain and can be implemented without additional hardware complexity in the terminal.**

Index Terms: **Frequency domain detection, Hermite pulses, multipath fading channel, pulse shape modulation (PSM), ranging, ultra wideband (UWB).**

I. INTRODUCTION

Pulse shape modulation is important because of its capacity to achieve high data rates compared with a single pulse system at the same pulse repetition frequency. Pulse shape modulation for ultra wideband (UWB) communications is proposed in [1], and achievable high data rates, by combining pulse shape modulation (PSM) with pulse position modulation (PPM), is reported in [2]. However, PSM has high detection complexity in time domain because of the following issues. First, the UWB channel models reported in [3] and [4] revealed that, depending on the transmitted signal pulsewidth, the arriving paths may not be resolvable, destructive addition of the multipath rays may occur, and the received UWB signal may contain components that greatly differ from the transmitted pulseshape. Then, in a multipath environment, a time domain detector may not be optimum even under perfect timing conditions. Second, detection of PSM pulses in time domain is severely affected by timing mismatches. The timing mismatching budget is mainly composed by the system clock drifts, the channel delay excess, accuracy of channel estimation, accuracy of adaptive finger allocation and system synchronization. The timing mismatching is considerable because of the short nature of UWB pulses.

Digital detection of PSM Hermite pulses in frequency domain is proposed in this paper. The proposed detection algorithm exploits the intrinsic orthogonality of the Hermite pulses Fourier transform along with low complexity frequency domain channel estimation. This algorithm let us profit from the energy of unresolved multipath components and relax timing matching complexity. The cost of implementing a digital receiver resides in the high conversion rate requirement on the analog to digital converter (ADC), although many techniques can be applied to alleviate this drawback. For example, a multi-channel approach is suggested in [5], where the sampling frequency is reduced by the number of channels and signal reconstruction is performed employing quadrature mirror filters. A different approach, where the receive signal projections on orthogonal spaces are sampled at reduced rates, is proposed in [6], and other approaches can be found in the references therein. On the other hand, higher sampling frequency ADCs based on superconducting schemes are under study [7], which in the future may allow high frequency digital receivers.

Related work is summarized as follows. Detection in frequency domain is studied in [8], where the method proposed in [6] is employed in order to relax the demands on the ADC processing capacity. In this approach, the receive signal is treated disregarding the transmitted pulseshape and the components of the receive signal are projected on an orthogonal basis of signals before digitization by a set of lower speed ADCs. Additionally, the Fourier transform of a filter, matched to the receive signal, is required for detection. This implies the necessity of channel estimation in order to define the impulse response of the matched filter and consequently the receiver complexity is increased. A channelized digital UWB receiver design can be found in [9], where the receiver signal is divided into a number of channels by a bank of continuous-time analog filters in order to smooth the ADC processing capacity requirements. Then, in the discrete-time domain the receive signal is synthesized for detection and complementarily the receiver signal can be down-converted to lower frequencies by heterodyning it with a locally generated signal. In this case, estimation of the receive signal is also required which under the multipath channel models studied in [3] and [4] imposes additional complexity. An all-digital frequency domain UWB receiver with channelized analog to digital conversion is reported in [10] including details about the design of the required channel estimation. A follow up, for a less efficient receiver employing 1 bit ADCs, is reported in [11], and the results in [12] complements the proposal. A digital approach for frequency domain detection employing channel equalization in the frequency domain is also studied in [13], where channel estimation is also required.

Manuscript received September 22, 2006; approved for publication by Xuemin Shen, Division II Editor, July 18, 2007.

A. Cartagena Gordillo is with the Division of Electrical and Computer Engineering, Yokohama National University, Japan, email: alex@kohnolab.dnj.ynu.ac.jp.

R. Kohno is with the Division of Electrical and Computer Engineering, Yokohama National University, Japan, email: kohno@kohnolab.dnj.ynu.ac.jp.

Ultra wideband antennas can be classified according to whether they distort the shape of the transmitted/received signal or not, they can be pulseshape distorting antennas and non-distorting antennas. With the aim of focusing on the techniques introduced in this study, the later type of antennas is assumed. It implies that the receive signal at the output of the receive antenna has the same pulseshape as the signal which feeds the transmitter antenna. Some examples of non-distorting antennas are analyzed and/or evaluated in [14]–[18].

In order to emphasize the proposals of this study, an impulse radio (IR) UWB system, which maps one pulse per symbol, in a single user environment is assumed.

Hereafter, this paper is organized into the following sections: In Section II, the receive UWB signal is defined, and pulse shape modulation and the frequency domain orthogonality of Hermite pulses are revisited. Section III describes the proposed frequency domain detection method and the proposed ranging algorithm. Computer simulations are presented in Section IV and our conclusions about this study complement this paper.

II. DEFINITIONS AND CONCEPTS

A. Pulse Shape Modulation

In pulse shape modulation, information bits 1 and 0 are represented by two different pulses. This idea can be extended to a N-ary modulation scheme using N pulse waveforms. Orthogonality among the pulseshapes is a desired quality for detection by a correlation-based receiver when signals are corrupted by AWGN.

B. Hermite Pulses and Their Frequency Domain Orthogonality

In this study, we employ Hermite pulses because of their exploitable orthogonality in the frequency domain besides their time domain orthogonality. Additionally, close forms of their Fourier transforms can be derived and employed for analysis. The nth Hermite pulse is defined as

$$\psi_n(t) = \frac{H_n(t)e^{-\frac{t^2}{2}}}{\sqrt{2^n n!\sqrt{\pi}}} \tag{1}$$

where $H_n(t)$ is the nth Hermite polynomial for $n \in [0, N-1]$. For further details, the reader is referred to [19] and [20].

Let $\Psi_n(\omega)$ be the nth Hermite pulse Fourier transform and N be the number of pulses in the alphabet. The time domain functions $\psi_n(t)$ form an orthonormal set and so do, although not evidently, their Fourier transforms.

Hermite pulses orthogonality in frequency domain can be summarized as in [21], but employing our nomenclature, it is mathematically expressed as

$$\Psi_n(\omega) = (-j)^n\sqrt{2\pi}\psi_n(\omega). \tag{2}$$

Table 1 shows the first four Hermite pulses along with their Fourier transforms, they are defined in terms of the angular frequency ω and scaled by $1/\sqrt{2\pi}$ aiming to show similitude between the time and the frequency domain expressions.

Table 1. Hermite pulses and their Fourier Transform.

n	$\psi_n(t)$	$\Psi_n(\omega)/\sqrt{2\pi}$
0	$\frac{e^{-t^2/2}}{\pi^{1/4}}$	$\frac{e^{-\omega^2/2}}{\pi^{1/4}}$
1	$\frac{t\sqrt{2}e^{-t^2/2}}{\pi^{1/4}}$	$\frac{-\omega\sqrt{2}e^{-\omega^2/2}}{\pi^{1/4}}$
2	$\frac{(2t^2-1)\sqrt{2}e^{-t^2/2}}{2\pi^{1/4}}$	$\frac{-(2\omega^2-1)\sqrt{2}e^{-\omega^2/2}}{2\pi^{1/4}}$
3	$\frac{t(2t^2-3)\sqrt{3}e^{-t^2/2}}{3\pi^{1/4}}$	$\frac{\omega(2\omega^2-3)\sqrt{3}e^{-\omega^2/2}}{3\pi^{1/4}}$

C. UWB receive signal

Let us assume a N-ary PSM UWB signal propagating through a multipath fading channel. The impulse response of the multipath channel is modeled as [3]

$$\varepsilon(t) = X\sum_{l=0}^{L}\sum_{k=0}^{K}\beta_{k,l}\delta(t - T_l - \tau_{k,l}) \tag{3}$$

where $\beta_{k,l}$ are the multipath gain coefficients, T_l is the delay of the lth cluster, $\tau_{k,l}$ is the delay of the kth multipath component relative to the lth cluster arrival time T_l, and X represents the log-normal shadowing.

The receive UWB signal of an individual pulse can be represented as the convolution of the transmitted pulse $\psi_n(t)$ with the channel impulse response $\varepsilon(t)$ plus noise,

$$r(t) = \psi_n(t)\varepsilon(t) + z(t) \tag{4}$$

assuming $z(t)$ to be zero-mean, white, and Gaussian distributed noise. Thus, replacing (3) into (4), the receive signal $r(t)$ can be expressed as

$$r(t) = X\sum_{l=0}^{L}\sum_{k=0}^{K}\beta_{k,l}\psi_n(t - T_l - \tau_{k,l}) + z(t). \tag{5}$$

The receive signal, after undergoing a sampling process, is defined as

$$r[m] = r(m\overline{T}), \qquad m = 1, 2, \cdots, M \tag{6}$$

where $\overline{T}$ is the sampling period and is reciprocal to the sampling frequency $f_s = 1/\overline{T}$. Next, the result of quantizing the sampled signal yields

$$\widehat{r}[m] = r[m] + e[m] \tag{7}$$

where $e[m]$ is the quantization error, which is thought to be an additive noise signal [22].

The discrete Fourier transform of the quantized signal in (7) is

$$R[w] = \Psi_n[w]\xi[w] + Z[w], \quad w = 1, 2, \cdots, W \tag{8}$$

where $\Psi_n[w]$ and $\xi[w]$ are the discrete Fourier transforms of the transmitted pulse $\psi_n(t)$ and the channel impulse response $\varepsilon(t)$ respectively, and $Z[w]$ is the discrete Fourier transform of the composed noise signal $z[m] + e[m]$. $\xi[w]$ is defined as

$$\xi[w] = X\sum_{l=0}^{L}\sum_{k=0}^{K}\beta_{k,l}e^{-j\omega(T_l+\tau_{k,l})} \tag{9}$$

where each individual term $\beta_{k,l}e^{-j\omega(T_l+\tau_{k,l})}$ is periodic in ω with a repetition rate proportional to $(T_l + \tau_{k,l})$.

III. SIGNAL PROCESSING IN FREQUENCY DOMAIN

A. Channel Estimation

Estimation of the propagation channel is necessary in order to extract the shape of the transmitted pulse from the receive signal. Its Fourier transform can be obtained from equation (8) and is mathematically described as

$$\xi[w] = \frac{R[w] - Z[w]}{\Psi_n[w]}. \tag{10}$$

However, since $Z[w]$ cannot be estimated, the complex valued multipath fading channel Fourier transform can be approximated by

$$\hat{\xi}^n[w] = \frac{R^n[w]}{\Psi_n[w]} \tag{11}$$

where the upper index n stands for the fact that the nth Hermite pulse has been used to estimate the channel. Assuming that P symbols per every nth pulse in the alphabet has been transmitted for channel estimation purposes, the average estimated value is given by

$$\hat{\xi}[w] = \frac{1}{NP}\sum_{p=1}^{P}\sum_{n=0}^{N-1}\hat{\xi}^n[w]. \tag{12}$$

B. Detection in Frequency Domain

Once again, we can invoke (8) to extract the transmitted pulseshape, and we can define an estimate of the transmitted pulse Fourier transform as

$$\hat{\Psi}[w] = \frac{R[w]}{\hat{\xi}[w]} \tag{13}$$

where we employ the estimated Fourier transform of the propagation channel $\hat{\xi}[w]$. Then, let us define the crosscorrelation of the estimated transmitted pulse and the nth receive template as

$$\chi(n) = \sum_{w=1}^{W}\overline{\Psi}_n[w]\Psi_n[w]\Delta \tag{14}$$

where Δ is the sample time which normalizes the results to unity, and

$$\overline{\Psi}_n[w] = \begin{cases} \mathrm{Re}(\hat{\Psi}[w]), & n = 0 \text{ or even}, \\ \mathrm{Im}(\hat{\Psi}[w]), & n = \text{odd} \end{cases} \tag{15}$$

where Re(.) and Im(.) stand for the functions which extract the real and imaginary components, respectively. Therefore, the detected transmit pulse can be defined as

$$\hat{n} = \max_n\{\chi(n)\}. \tag{16}$$

The block diagram of the proposed transmitter and receiver are shown in Figs. 1(a) and 1(b) respectively. The upper indexes $n \rightarrow$ even and $n \rightarrow$ odd imply that only even or only odd pulse orders are used as templates in those branches.

Additionally, since the Fourier transform of $-\psi_n(t)$ is $-\Psi_n(\omega)$, the extension from a N-ary orthogonal system to a $2N$-ary biorthogonal system is straightforward.

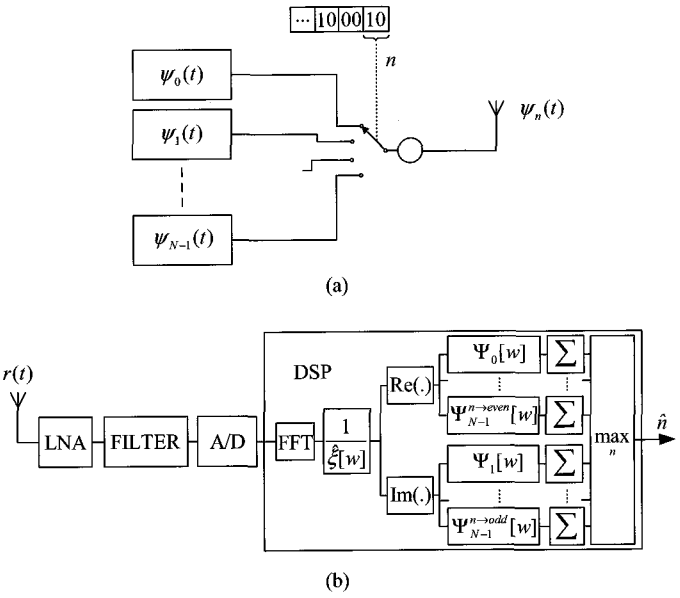

Fig. 1. Diagram of the proposed transceiver: (a) Transmitter and (b) receiver.

C. Cepstrum Algorithm

Cepstrum algorithm has been applied among other things to echo removal [23]. It permits to calculate accurately the time of occurrence of the echo signal. The complex cepstrum, $\overline{x}[m]$, of $x[m]$ is defined in [22], so that

$$x[m] \overset{\mathcal{F}}{\longleftrightarrow} X(e^{\jmath\omega}) = |X(e^{\jmath\omega})|e^{\jmath arg[X(e^{\jmath\omega})]}, \tag{17}$$

$$\overline{x}[m] \overset{\mathcal{F}}{\longleftrightarrow} \overline{X}(e^{\jmath\omega}) \tag{18}$$

where $\overset{\mathcal{F}}{\longleftrightarrow}$ denotes the bidirectional Fourier transform relationship between the time and frequency domain representations, and $\overline{X}(e^{\jmath\omega})$ is the natural logarithm of $x[m]$ Fourier transform. It is defined as

$$\overline{X}(e^{\jmath\omega}) = \log[X(e^{\jmath\omega})] = \log|X(e^{\jmath\omega})| + \jmath\arg[X(e^{\jmath\omega})] \tag{19}$$

where $\arg[X(e^{\jmath\omega})]$ denotes the continuous phase of $X(e^{\jmath\omega})$.

The position of the echo can be found as the highest amplitude component at a position different from the edges in $\overline{x}[m]$. Fig. 2(a) depicts the sampled and quantized receive signal $x[m]$, and Fig. 2(b) illustrates the corresponding cepstrum signal $\overline{x}[m]$ emphasizing the position of the echo signal. For further details, the reader is referred to [23].

D. Ranging

Ranging is performed by two transceivers in a sequence illustrated in Fig. 3. It is assumed that distance computations are carried out in receiver A, and operations occur after both transceivers have agreed on them.

For ranging calculation the receive signal $r^R[m]$ is defined as the sampled and quantized version of

$$r^R(t) = r(t - T1) + r(t - T3) \tag{20}$$

where $r(t)$ is defined in (5) and $T, T1, T2$, and $T3$ are multiples of the sampling time. Fig. 3(a) shows the signal stored by the terminal A in order to calculate the distance between terminals

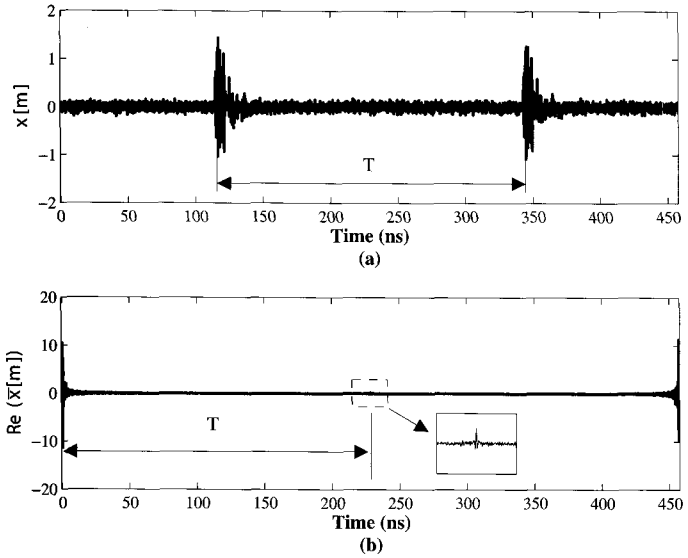

Fig. 2. (a) Receive signal with 5 dB of SNR and (b) cepstrum signal indicating the second pulse arrival time.

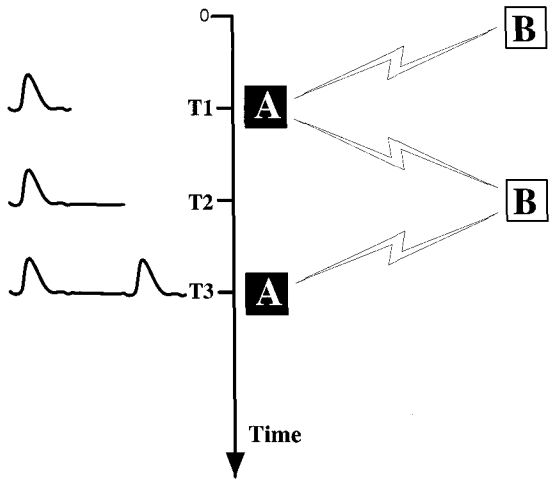

Fig. 3. Time of arrival calculation diagram. The calculation is done at transceiver A.

A and B. Additionally, it is assumed that the same pulseshape is employed during the operations, and the channel impulse response remains constant during the sampling of the receive signal $r^R[m]$.

Cepstrum algorithm let us determine the time difference $T = T3 - T1$ as illustrated graphically in Fig. 2(b). It is assumed that this time difference is composed by the propagation time between the antennas, T_{prop}, and the processing time for signal reception, T_{pr}, as well as signal transmission, T_{pt}, in terminals A and B. Then, defining $T_{pr} = T_{pr}^A = T_{pr}^B$ and $T_{pt} = T_{pt}^A = T_{pt}^B$, the propagation time between antennas is given by

$$T_{prop} = \frac{T - T_{pr}^B - T_{pt}^A - T_{pt}^B}{2} = \frac{T - T_{pr} - 2T_{pt}}{2}. \quad (21)$$

Assuming that T_{pr} and T_{pt} are known, the calculated distance between the terminals A and B is approximated by

$$d \approx c\, T_{prop} \quad (22)$$

where c is the assumed propagation velocity.

IV. SIMULATION RESULTS

Except in Section IV-D, the channel models $CM1$ and $CM2$ reported in [3] are employed through the computer simulations, and in all but Section IV-E four pilot symbols per every pulse in the set are transmitted for channel estimation purposes. A 4-ary system, employing the first four Hermite pulses, is employed and no transmission diversity is assumed i.e. transmission of one pulse per symbol. Additionally, ideal RF front-end signal processing is assumed at the receiver side.

A. Sampling Frequency

In order to determine the minimum number of $\overline{W}$ samples per pulsewidth for a 4-ary system based on the first four Hermite pulses, we computed the standard deviation of the autocorrelation vector of the employed pulses.

$$CORR_{STD} = \sum_{n=0}^{N-1} \sum_{\bar{w}=-\frac{Band}{2(\overline{W}-1)}}^{\frac{Band}{2(\overline{W}-1)}} \psi_n[\bar{w}]\psi_n[\bar{w}],\ \bar{w} = 1, 2, \cdots, \overline{W} \quad (23)$$

where $Band$ is a zero-centered portion of the Hermite pulses, which is graphically depicted in Fig. 4(a) and is included as a variable in the ordinate axis in Fig. 4(b). $CORR_{STD}$ is plotted in Fig. 4(b) in function of $Band$ and the number of samples $\overline{W}$, darker areas represent low values of standard deviation, i.e., the autocorrelation values are closer to unity. Therefore, good values of $Band$ and $\overline{W}$ can be obtained from any point laying into the darker area. Fig. 4(a) illustrates the Hermite pulses as functions which are neither time nor frequency domain representations. The goal is to show the relationship between the considered portion of the first four Hermite pulse and its minimum number of samples.

Even though it is possible to get high values of $CORR_{STD}$ with low values of $Band$, regarding the signal spectrum, it implies filtering the receive signal at those values before A/D conversion. This filtering distorts the shape of the receive signal and degrades performance. Therefore, the value of $Band$ should be high enough to guarantee non-distortion of the sampled signal. Then, in this study we assume a value of $Band = 8$. On the other hand, the number of samples is required to be an odd number because of the high importance of the sample at the origin of the abscissas axis in Fig. 4(a). Therefore, in this study we assume $\overline{W} = 17$.

B. Detection of PSM

The proposed digital receiver with 8 quantization bits and 17 samples per pulse is employed. The symbol error rate against the signal to noise ratio results for the proposed system is illustrated in Fig. 5. These results are product of the multipath-channel equalization carried out at the receiver and they are better than a pure AWGN channel case, such as in [20], because of the digital nature of our receiver, which accounts for the influence of AWGN at sampling time.

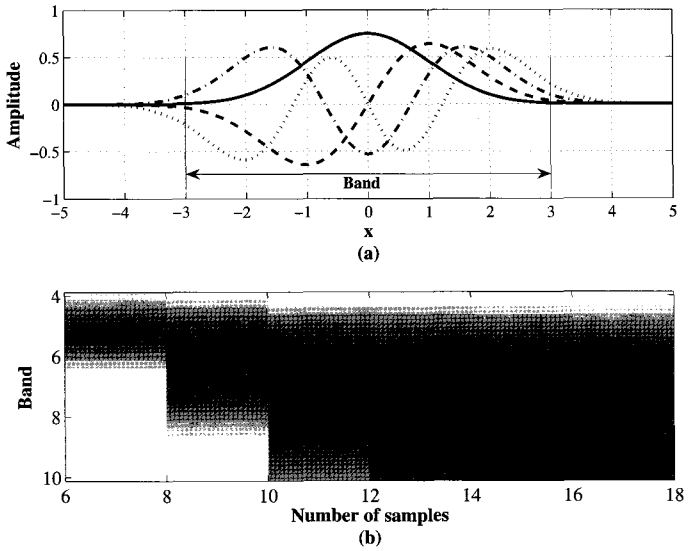

Fig. 4. Minimum number of samples for the first four Hermite pulses illustrated in (a). The darker areas in (b) represent lower error on the autocorrelation for a given number of samples within a determined value of $Band$.

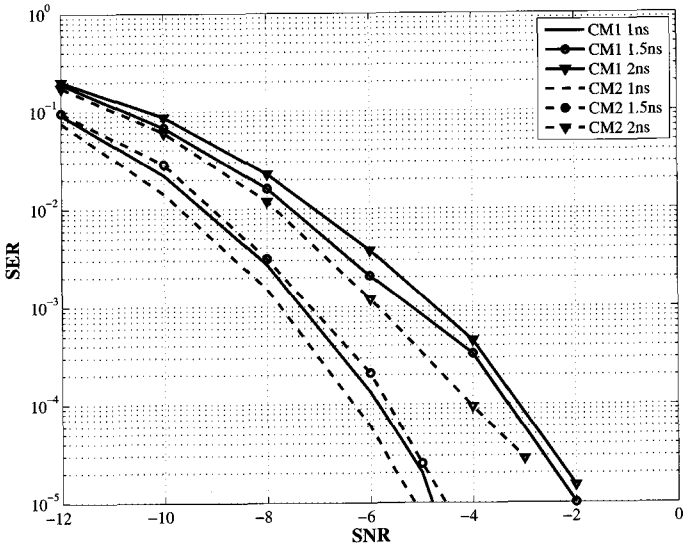

Fig. 5. Performance of the proposed system employing the first four Hermite pulses in a 4-ary UWB PSM system, with pulsewidth values of 1 ns, 1.5 ns, and 2 ns, and eight quantization bits. They are evaluated in the multipath channel models CM1 and CM2.

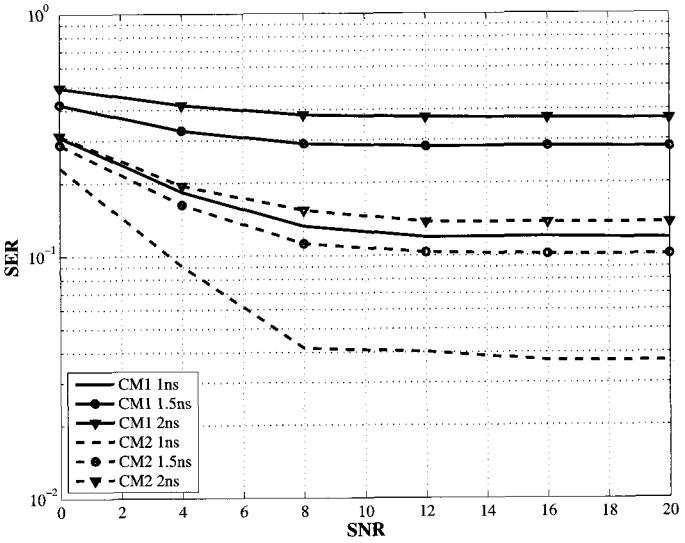

Fig. 6. Performance of a time domain rake receive which employs the first four Hermite pulses in a 4-ary UWB PSM system, with pulsewidth values of 1 ns, 1.5 ns, and 2 ns evaluated through the multipath channel models CM1 and CM2.

The performance of a time domain rake receiver with maximum ratio combiner (MRC) is plotted for comparison purposes in Fig. 6. The complexity of this system is composed by channel estimation, selection of the strongest and resolvable paths, ideal timing matching, adaptive finger correlator delay, weighting of the correlation outputs and accumulation of the results. Different from a single-pulse rake receiver, a PSM rake receiver cannot allocate fingers separated in time by a pulsewidth. Because of its maximum likelihood decision among N candidates, it needs to allocate fingers adaptively in order to correlate resolvable arriving paths.

Both systems are evaluated for different values of pulsewidth, and the results show that shorter pulses have better performance than longer ones. This is because with shorter pulses the number of resolvable multipath components is higher. Similar results were reported for a single pulse rake receiver in [24].

In all cases, the performance of the systems evaluated through the channel model CM2 is better than the one with the channel model CM1. It is explained as the channel model CM2 has higher number of multipath components (multipath arrivals that are within 10 dB of the peak multipath component) [3], and arrival paths are more sparse than in channel model CM1.

C. Mistiming Effects

The effect of jitter in the detection performance of the proposed system is shown in Fig. 7. Jitter affects every sample in the A/D conversion process and is modeled as an independent and identically distributed (i.i.d.) random variable which is zero-mean Gaussian-distributed in the range of $\{-30$ ps, 30 ps$\}$ [25]. Jitter effects are evaluated in a system with 2 ns pulsewidth because it has the worst performance in the previous section and it has the lowest sampling frequency (8 GHz). The jitter-affected performance curves show slightly better performance in some ranges of signal to noise ratio, this is because jitter can be seeing as an additional source of additive noise, which can be beneficial against quantization errors since it behaves as dither. To show our point, an extra performance curve of the proposed system whose receive signal is dithered with an additional noise component that is equally distributed in the range $[-0.5\ LSB, 0.5\ LSB]$, where LSB stands for least significant bit, is shown in Fig. 7. This additional curve does not have the intention to model precisely the effects of jitter, but to show the effects of an extra source of noise, which can be compared with the jitter effects and explain the results in Fig. 7.

D. Frequency Dependency

From the three propagation mechanisms: line of sight, reflection and diffraction, only the later one causes the strength of the diffraction field to be frequency dependent. The frequency dependency can be used to trace, detect, and characterize a ray path [26]. The UWB propagation channel frequency dependence

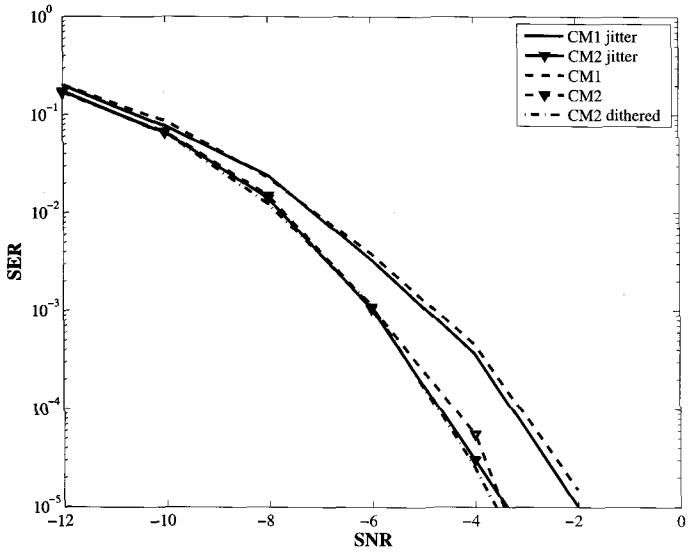

Fig. 7. Effects of jitter on the proposed detection scheme.

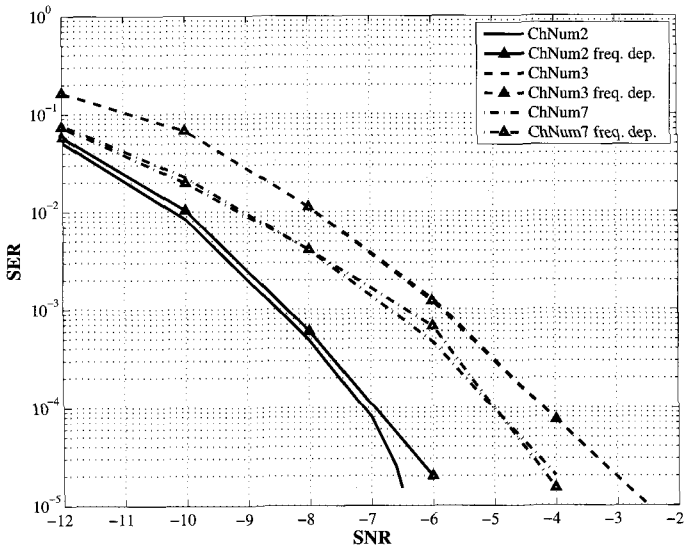

Fig. 8. Frequency dependency influence on the performance of the proposed system. It is evaluated for different channel models from [4].

pathloss $PL(f)$ is modeled in [4] along with distance dependence pathloss $PL(d)$ as $PL(f,d) = PL(f)PL(d)$, where $\sqrt{PL(f)} \propto f^{-\kappa}$ and κ is a frequency dependence factor. The frequency dependence factor κ is determined by the geometric configurations of the objects, for a corner, like a corner of a desk, the frequency dependency is $\kappa = -1$ [26]. The frequency dependence of a multiple diffraction ray can be modeled by multiplying the frequency dependence of all the encountered scattering mechanisms [27], e.g., a ray which is first diffracted by a wall edge ($\kappa = -0.5$) and then by another wall edge ($\kappa = -0.5$), has frequency dependence equal to $1/\omega$ ($\kappa = -1$) [26]. Therefore, an arriving ray with a frequency dependence coefficient κ can be product of a single diffraction scatterer or one composed by the frequency dependence coefficient product of more than one scatterer. In the channel models described in [4], it is assumed that pulse distortion for all the paths are identical, but the statistical model for the general case (independent values of κ per path) is currently not available [28]. Different from the channel models in [3], the models employed in this section are complex-valued and are denoted as ChNum2, ChNum3, and ChNum7, they correspond to NLOS residential, LOS office and LOS industrial, and they were selected because of the difference of their factor κ, which are 1.53, 0.03, and -1.1 respectively [29]. Fig. 8 depicts the performance difference introduced by the inclusion or not of the frequency dependence pathloss component $PL(f)$ (denoted as Freq. Dep.) in the evaluations. It is appreciated that the larger the value of $|\kappa|$ the higher the performance degradation and for ChNum3 the difference between the frequency dependent and non-frequency dependent performance plots are indiscernible, these results are in accordance with the exponential influence of κ in the definition of $PL(f)$. In all cases, the pulsewidth is $2ns$.

E. Ranging

The probability of distance estimation error against the signal to noise ratio is shown in Fig. 9 for channel models CM1 and CM2. The accuracy of the distance estimation depends on the sampling time, which for a 2 ns pulsewidth is assumed to

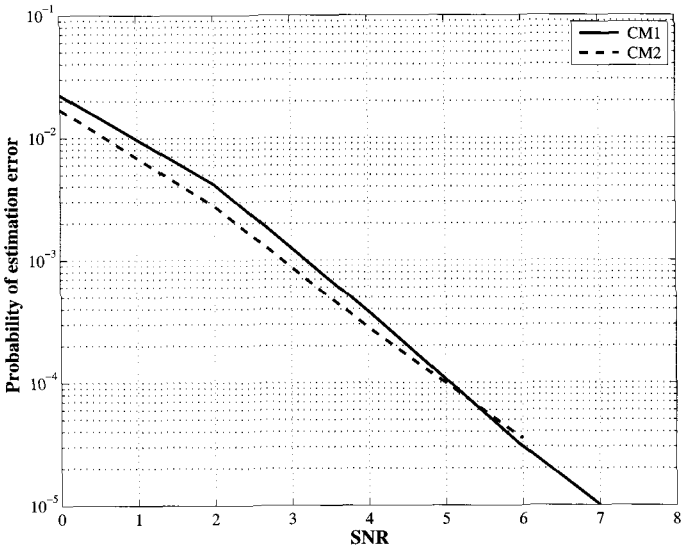

Fig. 9. Distance estimation probability of error for the proposed method employing the Cepstrum algorithm.

be 0.125 ns, and with a velocity of propagation equal to the velocity of light the minimum discernible distance is 3.75 cm. It is necessary to include an exception in the implementation of equation (19) in order to avoid taking the logarithm of zero valued arguments; it can be done replacing them with very small numbers.

V. CONCLUSION

Exploiting the orthogonality of the Hermite pulses Fourier transform, we propose a frequency domain detection system. This frequency domain technique permits the detection of orthogonal UWB PSM Hermite pulses in a maximum likelihood way even when they operate in severe multipath fading channel conditions. The proposed systems and the presented rake receiver have better performance when the non-line of sight channel model CM2 is employed. This is because the arriving rays in the CM2 channel model are sparse, while the more concen-

trated rays in the CM1 model generates inter-path interference, which distorts the pulseshape more severely. Additionally, the number of paths within the 10 dB of the peak multipath arrival is greater in the CM2 channel model. A novel ranging method based in the Cepstrum algorithm is additionally proposed, this algorithm can be implemented without increasing the hardware complexity of the terminals. The costs of the proposed systems are translated into the increased capacity demand on the ADC.

REFERENCES

[1] M. Ghavami, L. B. Michael, and R. Kohno, "Hermite function based orthogonal pulses for ultra wideband communications," in *Proc. Wireless Personal Multimedia Communications (WPMC)*, Alborg, Denmark, Sept. 2001, pp. 437–440.

[2] C. J. Mitchell and R. Kohno, "Combined pulse shape and pulse position modulation for high data rate transmissions in UWB communications," in *Proc. International Workshop on Ultra Wideband Systems (IWUWBS)*, Oulu, Finland, June 2003.

[3] J. Foerster, "Channel modeling sub-committee report final," IEEE P802.15 Wireless Personal Area Networks, IEEE P802.15-02/490r1-SG3a, Feb. 2003.

[4] A. F. Molisch, "802.15.4a channel model subgroup final report," IEEE P802.15 Wireless Personal Area Networks, IEEE P802.15-04-0535-00-004a, Sept. 2004.

[5] C. Gangyaokuang and S. Zhonglianglu, "A way of multi-channel A/D for UWB signal," in *Proc. IEEE National Aerospace and Electronics Conf. (NAECON)*, Dayton, Ohio, USA, May 1995, pp. 206–209.

[6] S. Hoyos, B. M. Sadler, and G. R. Arce, "Analog to digital conversion of ultra-wideband signals in orthogonal spaces," in *Proc. IEEE Conference on Ultra Wideband Systems and Techniques (UWBST)*, Reston, Virginia, USA, Nov. 2003, pp. 47–51.

[7] F. Furuta, K. Saitoh, and K. Takagi, "Design of front-end circuit for superconductive A/D converter and demonstration of operation up to 43 GHz," *IEEE Trans. Appl. Superconduct.*, vol. 14, pp. 40–45, Mar. 2004.

[8] S. Hoyos, B. M. Sadler, and G. R. Arce, "Ultra-wideband multicarrier communication receiver based on analog to digital conversion in the frequency domain," in *IEEE Wireless Commun. and Netw. Conf. (WCNC)*, New Orleans, LA, USA, Mar. 2005, pp. 782–787.

[9] W. Namgoong, "A channelized digital ultra wideband receiver," *IEEE Trans. Wireless Commun.*, vol. 2, pp. 502–510, May 2003.

[10] H.-J. Lee, D. S. Ha, and H.-S. Lee, "A frequency-domain approach for all-digital CMOS UWB wideband receivers," in *Proc. IEEE Conf. on Ultra Wideband Systems and Techniques (UWBST)*, Reston, Virginia, USA, Nov. 2003.

[11] ——, "Toward digital UWB radios: Part I - Frequency domain UWB receiver with 1 bit ADCs," in *Proc. Int. Workshop on Ultra Wideband Systems Joint with Conf. on Ultra Wideband Systems and Technologies (Joint UWBST & IWUWBS)*, Kyoto, Japan, May 2004.

[12] ——, "Toward digital UWB radios: Part II - A system design to increase data throughput for a frequency domain UWB receiver," in *Proc. Int. Workshop on Ultra Wideband Systems Joint with Conf. on Ultra Wideband Systems and Technologies (Joint UWBST & IWUWBS)*, Kyoto, Japan, May 2004.

[13] T. Bianchi and S. Morosi, "Frequency domain detection for ultra-wideband communications in the indoor environment," in *Proc. IEEE Int. Symp. on Spread Spectrum Techniques and Applications (ISSSTA)*, Sydney, Australia, Sept. 2004, pp. 493–497.

[14] J. R. Andrews, "UWB signal sources, antennas & propagation," 2003, extended Version of the paper at 2003 IEEE Tropical Conf. on Wireless Commun. Technology. [Online]. Available: http://www.ccsds.org/documents/pdf/CCSDS-101.0-B-4.pdf

[15] H. G. Schantz, "Dispersion and UWB Antennas," in *Proc. Int. Workshop on Ultra Wideband Systems Joint with Conf. on Ultra Wideband Systems and Technologies (Joint UWBST & IWUWBS)*, Kyoto, Japan, May 2004, invited Talk.

[16] A. H. Mohammadian, A. Rajkotia, and S. S. Soliman, "Characterization of UWB transmit-receive antenna system," in *Proc. IEEE Conf. on Ultra Wideband Systems and Techniques (UWBST)*, Virginia, USA, Nov. 2003.

[17] J. Powell and A. Chandrakasan, "Differential and single ended elliptical antennas for 3.1-10.6 GHz ultra wideband communication," in *Antennas and Propagation Society Int. Symp., IEEE*, Monterrey, California, USA, June 2004.

[18] S. Nikolaou, L. Marcaccioli, G. E. Ponchak, J. Papapolymerou, and M. M. Tentzeris, "Conformal double exponentially tappered slot antennas (DETSA) for UWB communications systems' front-ends," in *Proc. IEEE Int. Conf. on Ultra-Wideband (ICU)*, Zurich, Switzerland, Sept. 2005.

[19] A. Cartagena Gordillo, G. T. F. de Abreu, and R. Kohno, "Band-limited frequency efficient orthogonal pulse shape modulation for UWB communications," in *Proc. IEEE Int. Symp. on Spread Spectrum Techniques and Applications (ISSSTA)*, Sydney, Australia, Sept. 2004, pp. 498–502.

[20] G. T. F. de Abreu, C. J. Mitchell, and R. Kohno, "On the design of orthogonal-shape modulation for UWB systems using Hermite pulses," *Journal of Commun. and Networks*, vol. 5, pp. 100–124, Dec. 2002.

[21] G. G. Walter, *Wavelets and Other Orthogonal Systems With Applications*. Boca Raton, FL: CRC Press, 1994.

[22] A. V. Oppenheim and R. W. Schafer, *Discrete-Time Signal Processing*, 2nd Ed. Upper Saddle River, NJ: Prentice Hall, 1998.

[23] R. W. Schafer, "Echo removal by discrete generalized linear filtering," Ph.D. dissertation, Massachusetts Institute of Technology, Cambridge, Jan. 1968.

[24] M. A. Rahman, S. Sasaki, J. Zhou, and H. Kikuchi, "On rake reception of ultra wideband signals over multipath channels from energy capture perspective," *IEICE TRANS. FUNDAMENTALS. Special Section on Ultra Wideband Systems*, vol. E88, pp. 2339–2349, Sept. 2005.

[25] I. Guvenc and H. Arslan, "Performance analysis of UWB systems in the presence of timing jitter," *Journal of Commun. and Networks*, vol. 6, pp. 182–191, June 2004.

[26] R. C. Qiu and I.-T. Lu, "Wideband wireless multipath channel modeling with path frequency dependence," in *IEEE Int. Conf. on Commun. (ICC)*, Dallas, TX, June 1996.

[27] R. C. Qiu, "A study of the ultra-wideband wireless propagation channel and optimum (UWB) receiver design," *IEEE J. Sel. Areas Commun.*, vol. 20, pp. 1628–1637, Dec. 2002.

[28] R. C. Qiu, J. Q. Zhang, and N. Guo, "Detection of physics-based ultra-wideband signals using generalized rake with multiuser detection (MUD) and time-reversal mirror," *IEEE J. Sel. Areas Commun.*, vol. 24, pp. 724–730, Apr. 2006.

[29] S. Xu, K. C. Wee, B. Kannan, and F. Chin, "Channel-model-matlab-code-ver-9.zip," IEEE 802.15-4a, Tech. Rep. 15-05-0114-00-004a, Feb. 2005. [Online]. Available: ftp://ftp.802wirelessworld.com/15/05/

Alex Cartagena Gordillo was born in Puno, Peru in March 1970. He received his B.E. in electronics engineering from San Agustin State University of Arequipa - Peru in 1994; he finished studies of Second Specialization in Systems Engineering in the same university in 1999. In 2003, he received his M.E. in electrical and electronic engineering from The University of Tokushima - Japan. Currently, he is working towards his Ph.D. degree in the Division of Electrical and Computer Engineering, Faculty of Engineering of Yokohama National University. He is interested in ultra wideband, software defined radios, and spectral analysis.

Ryuji Kohno received the B.E. and M.E. degrees in computer engineering from Yokohama National University in 1979 and 1981, respectively and the Ph.D. degree in electrical engineering from the University of Tokyo in 1984. He has been a professor in the Division of Electrical and Computer Engineering, Yokohama National University (YNU) since 1998. He was a director of SONY Advanced Telecommunications Laboratory during 1998–2002 and a director of the UWB Technology institute of National Institute of Information and Communications Technology (NICT), and a president of 21st century COE (center of excellence) of Creation of Future Social Infrastructure Based on Information Telecommunications Technology in YNU during 2002–2007. Currently he is a director of the Medical Information and Communication Technology Center in Yokohama National University as well as a director of the Medical ICT institute of the NICT. He has covering a wide area of information theory and its applications such as coding theory, spread spectrum system, space-time coding and signal processing, SDR (software defined radio), UWB (ultra wideband), and their applications to medical care, intelligent transport systems (ITS) and so on. He was elected to be a member of the Board of Governors of the IEEE

Information Theory Society twice on 2000 and 2002. He was an editor of the IEEE Transactions on Information Theory during 1995–1998, currently is that of the IEEE Transactions on Communications since 1994 and that of the IEEE Transactions on Intelligent Transport Systems (ITS) since 2000. He is a fellow of IEICE (Institute of Electronics, Information, Communications Engineers), and has been a vice-president of Engineering Sciences Society of IEICE, the chairman of the IEICE Technical Committee on Spread Spectrum Technology, that on ITS, and that on SDR. Currently he is an editor-in chief of the IEICE Transactions on Fundamentals of Electronics, Communications, and Computer Sciences, and the vice-president of SITA (Society of Information Theory and its Applications). He was awarded IEICE Greatest Contribution Award and NTT DoCoMo Mobile Science Award in 1999 and 2002, respectively.